Comparison Study of the Flux Pinning Enhancement of $YBa_2Cu_3O_{7-\delta}$ Thin Films With $BaHfO_3 + Y_2O_3$ Single- and Mixed-Phase Additions

Mary Ann Sebastian, Bibek Gautam, Charles R. Ebbing, George Y. Panasyuk, Michael A. Susner, Jijie Huang, Wenrui Zhang, Haiyan Wang, Judy Z. Wu, and Timothy J. Haugan

***Abstract*—Incorporating nano-scale insulating phases to $YBa_2Cu_3O_{7-\delta}$ (YBCO) superconductor thin films enhances flux pinning by combining different pinning mechanisms, which in turn increases the current density. This research explores the effects of addition of the non-reactive phases of barium hafnate (BHO) and yttrium oxide Y_2O_3. Pulsed laser deposition (PLD) produces thin films on $SrTiO_3$ (STO) substrates at various deposition temperatures ranging from 790 °C to 840 °C. PLD target compositions vary the volume percent of BHO from 2 to 6 vol% while maintaining 3 vol% Y_2O_3 and the remaining vol% YBCO. Examining the microstructure through SEM, TEM, and XRD analyses provides insight into the impact of the additions of BHO and Y_2O_3 on the YBCO thin films' magnetic and transport current densities measured with an applied field parallel to the *c* and *ab* directions, and on the films' critical temperature measurements. The Y_2O_3 additions decrease the variability in the current density between the *c* and *ab* directions, which is an important aspect to consider in applications, such as for HTS wires for motors.**

***Index Terms*—Critical current density, Flux pinning, Superconducting thin films, Type II superconductors, Yttrium barium copper oxide.**

Manuscript received December 12, 2018; accepted January 8, 2019. Date of publication January 10, 2019; date of current version March 1, 2019. This work was supported in part by AFRL/Aerospace Systems Directorate and the Air Force Office of Scientific Research under Grant LRIR #14RQ08COR and Grant LRIR #18RQCOR100) and in part by ARO under Grant W911NF-16-1-0029. The work of H. Wang was supported by the National Science Foundation (NSF) under Grant DMR-1565822 for TEM courtesy. The work of J. Wu was supported by NSF under Grant DMR-1337737 and Grant DMR-1508494 for angular current density measurements courtesy. The work of M. A. Susner was supported by the National Research Council. *(Corresponding author: Mary Ann Sebastian.)*

M. A. Sebastian and C. R. Ebbing are with the University of Dayton Research Institute, University of Dayton, Dayton, OH 45469 USA (e-mail: mary_ann.sebastian.1.ctr@us.af.mil; charles.ebbing.ctr@us.af.mil).

B. Gautam and J. Z. Wu are with the Department of Physics and Astronomy, University of Kansas, Lawrence, KS 66045 USA (e-mail: gautbibe@ku.edu; jwu@ku.edu).

G. Y. Panasyuk and M. A. Susner are with UES, Beavercreek, OH 45432 USA (e-mail: george.panasyuk.1.ctr@us.af.mil; michael.susner.ctr@us.af.mil).

J. Huang W. Zhang, and H. Wang are with the School of Materials Engineering, Purdue University, West Lafayette, IN 47907 USA (e-mail: haun1027@purdue.edu; zhwrican@gmail.com; hwang00@purdue.edu).

T. J. Haugan is with the Air Force Research Laboratory RQQM Wright Patterson Air Force Base, Dayton, OH 45431 USA (e-mail: timothy.haugan@us.af.mil).

Color versions of one or more of the figures in this paper are available online at http://ieeexplore.ieee.org.

Digital Object Identifier 10.1109/TASC.2019.2892324

I. Introduction

ADDING nano-scale size insulating phases to $YBa_2Cu_3O_{7-\delta}$ (YBCO) thin films improves flux pinning, which in turn improves current densities. These phases may be incorporated by various means and as different morphologies; each of which provides pinning benefits for different operating conditions [1]. From Matsumoto's work, it is known that these morphologies can be categorized as one, two, and three dimensional artificial pinning centers (1D - APC, 2D - APC, 3D -APC). 1D - APC's display linear defects, from addition of $BaSnO_3$ (BSO), $BaZrO_3$ (BZO), and $Ba_2Y(Nb,Ta)O_6$ (BYNTO) nanorods for example. 2D – APC's display planar defects that result from low angle grain boundaries and large precipitate surfaces. Y_2O_3 and Y211 nanoparticles are examples of 3D – APC's [2]–[7]. In reference to the periodic table, Hafnium lies below Zirconium, prompting interest to explore the addition of $BaHafO_3$ (BHO) nano-rods to YBCO thin films. BHO also possesses a smaller lattice mismatch with YBCO, in comparison to BZO, which is an important consideration in the epitaxial growth of superconducting thin films [8]. At the time, our research group was aware of four published papers that investigated the addition of BHO to YBCO films: S. Sato researched 1.5 and 3.0 wt.% BHO additions in June 2013, and from the same research group, M. Watanebe in 2014 researched 0.5,1.0,.and 2.0 wt.% BHO additions [9], [10]. M. Sieger in June 2015 studied 2, 4, and 6 mol% BHO additions on both Ni9W buffered tapes and STO substrates [11]. T. Matsushita compared with 3.5 mol% BHO to 3.5 mol% BZO doped GdBCO on IBAD substrates [12].

This paper explores the addition of 2, 4, and 6 vol.% BHO in conjunction with 3 vol.% Y_2O_3. This paper then goes on to directly compare the 2 vol.% BHO + 3 vol.% Y_2O_3 double doped film to a film doped only with 2 vol.% BHO. Our collected research shows the effect of double doping with two non-reacting insulated phases on the current density and flux pinning landscape through current density measurements, XRD analysis, and SEM and TEM imaging. A theoretical temperature dependence model of the isotropic weak and anisotropic strong pinning contributions developed by Blatter and Nelson was used to isolate the two different pinning mechanisms for the current density data measured with a field H // c direction of 3 Tesla at 77, 65, 60, 50, 30, 20, 10, and 5 K with the vsm-ppms [8], [13]–[16].

TABLE I
PLD TARGET COMPOSITIONS

Target	YBCO (vol. %)	BHO (vol. %)	Y_2O_3 (vol. %)
TS204	95	2	3
TS205	93	4	3
TS206	91	6	3
TS208	98	2	

II. EXPERIMENTAL

A. Target Preparation

A solid state processing method was used to produce targets from dried commercial powders of YBCO, $BaCO_3$, HfO_2, and Y_2O_3. $BaHfO_3$ powder was synthesized in a two -step process in a box furnace, by reacting barium carbonate and hafnium oxide (1)–(3). Initially the temperature was ramped at 150 °C/hr to 1000 °C and held for 2 hours. This converts the barium carbonate to barium oxide. This is followed by ramping at 150 °C/hr to 1400 °C, which is held for 8 hours, during which time the barium oxide reacts with the hafnium oxide to form barium hafnate (BHO) [17].

$$BaCO_3\,(s) \rightarrow BaO\,(s) + CO_2\,(g) \quad (1)$$

$$BaO\,(s) + HfO_2\,(s) \rightarrow BaHfO_3\,(s) \quad (2)$$

$$BaCO_3\,(s) + HfO_2\,(s) \rightarrow BaHfO_3\,(s) + CO_2\,(g) \quad (3)$$

The dried powders were then pressed and sintered until the final percent densities of the four targets ranged between 87.40% and 92.10%. For additional processing details the reader is referred to reference [8]. Compositions of the targets can be found in Table I.

B. Thin Film Production via Pulsed Laser Deposition (PLD)

Pulsed laser deposition (PLD) with the previously mentioned targets was utilized to produce the thin films on $SrTiO_3$ (STO) substrates. Details of the PLD procedure can be found in reference [8].

C. Film Characterization

Films were characterized by measuring film thickness, imaging the films' surfaces with a scanning electron microscope, imaging the films' cross sections with a transmission electron microscope, determining lattice parameters with x-ray diffraction analysis, and measuring magnetic current densities (J_{cm}), angular transport current densities (J_{ct}), and corresponding pinning forces, along with respective critical temperatures. Specific details in regards to the type of equipment utilized and pertinent procedures can be found in references [8] and [18]–[21].

III. RESULTS AND DISCUSSION

Thin films on STO substrates were deposited via PLD utilizing the 4 vol.% BHO + 3 vol.% Y_2O_3 target, at deposition temperatures ranging from 790 °C to 840 °C. From Fig. 1(a), (b) which show the magnetic current density measurements at 65 K and 5 K with applied magnetic field up to 9 T, the optimum deposition temperature occurs at 790–810 °C. In Fig. 1(c), the magnetic current density at 65 K and 5 K with applied magnetic field up to 9 T was measured comparing films deposited from targets varying the vol.% of BHO from 2, 4, and 6% and maintaining Y_2O_3 at 3 vol.%, and shows the optimum current

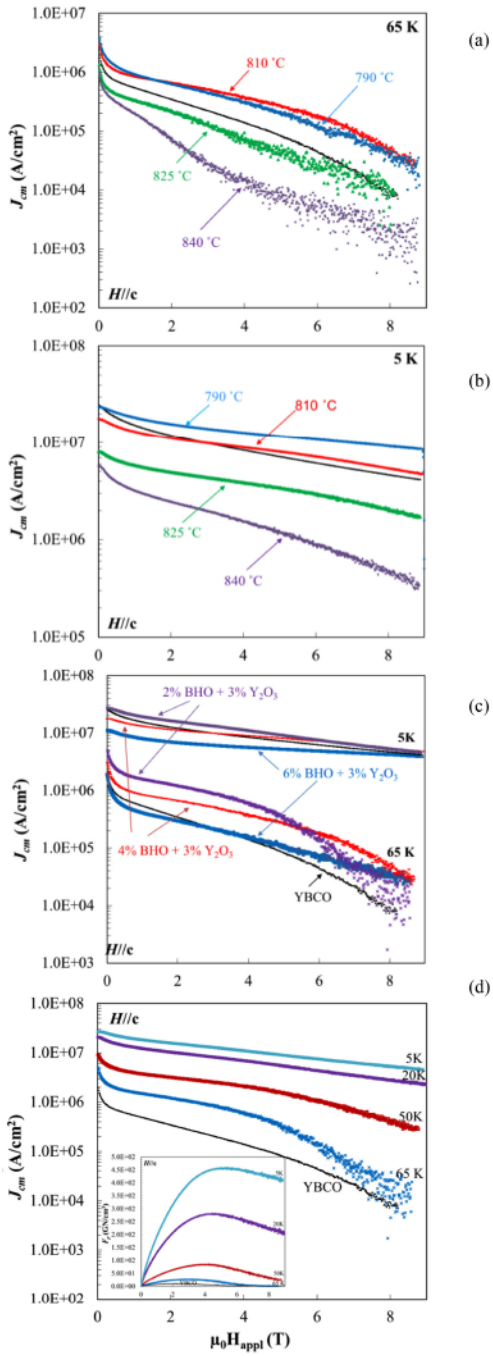

Fig. 1. Current density vs applied field at 65K and 5K for (a), (b) 4 vol.% BHO + 3 vol.% Y_2O_3 doped YBCO films deposited at various deposition temperatures, (c) 2, 4, and 6 vol.% BHO+ 3 vol.% Y_2O_3 doped YBCO films deposited at 810 °C, (d) 2 vol.% BHO+ 3 vol.% Y_2O_3 doped YBCO film measured at 5 K–65 K with corresponding pinning force inset graph. The black curves represent YBCO film current density measurements for reference.

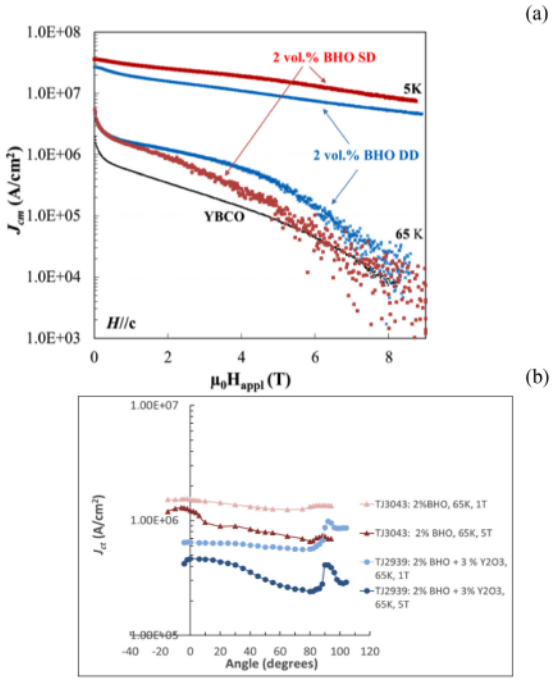

Fig. 2. Comparison of J_{cm} vs applied field at 65K and 5K for (a) 2 vol.% BHO and 2 vol.% BHO + 3 vol.% Y_2O_3 doped YBCO films. (b) Angular J_{ct} vs. applied field for single and double doped 2 vol.% BHO YBCO films.

density is attained for the 2 vol.% double doped BHO film. For reference, the measured film thicknesses were 158, 162, and 196 nm for the 2, 4, and 6 vol.% double doped BHO + Y_2O_3 respectively. The single doped 2 vol.% BHO film was 168 nm thick. Fig. 1(d) shows magnetic current densities measured at 65, 50 20, and 5 K for the optimized composition of 2 vol.% BHO double doped film, and the corresponding pinning force curves. The magnetic current densities at 65 K and 5 K and the angular transport current densities at 65 K for the optimized double doped (DD) 2 vol.% BHO film compared to the single doped (SD) 2 vol.% film are shown in Fig. 2(a). This comparison shows that the addition of 3 vol.% Y_2O_3 provides additional pinning force and higher current density at 65 K, whereas at 5 K, the SD 2 vol.% BHO doped YBCO film gives the highest attainable current densities. An important aspect to consider is also the response of current density measured to the direction of the applied field. Thus far, results discussed pertained to the field being parallel to the c-direction. In Fig. 2(b), the angle of the field is changed from being parallel to the c direction, to parallel to the ab direction, with measurements taken at 65 K, 1 T and 5 T. The pinning effect of the BHO nanorods is evidenced by the higher current density at H//c for the 2 vol.% SD BHO film at 65 K, 5 T, when compared to H//ab. Also, at 65 K and 5 T, the addition of Y_2O_3 resulted in films with a more uniform response to the angle of applied field, with the current density at H//c similar in magnitude to the current density at H//ab. This illustrates two competing figure of merits, such that in order to achieve less variation in current density with varying direction of the applied field the highest current density attainable needs to be sacrificed.

Table II lists the critical temperatures which were also measured with the vsm-ppms, for the doped films and for a YBCO

TABLE II
T_c 's OF SINGLE AND DOUBLE BHO DOPED YBCO FILMS

	YBCO	2% DD BHO	4% DD BHO	6% DD BHO	2 % SD BHO
T_c (K)	89.2	88.4	87.1	85.8	88.9

un-doped film. As expected, T_c did decrease as the amount of dopants increased, due to the dopants effects on the film microstructure. The greatest decrease occurred for the 6 vol.% BHO + 3 vol.% Y_2O_3 doped YBCO film.

While each of the various dopant level films studied grew epitaxially, as evidenced from the xrd 2θ– omega scans shown in Fig. 3(a), the effect on the microstructure of the increased dopant concentration is evidenced in the FWHM results from the xrd rocking curves on the YBCO (005) peak (Table III), and also in the SEM imaging and in the TEM analysis in Fig. 3(b)–(c). Increased doping resulted in more surface pores and defects, when compared to the undoped YBCO film. Also, whereas the 2% BHO SD film contained BHO nano-rods which are clearly seen in the TEM imaging, and which were responsible for the high J_c with the field parallel to the c direction, the addition of Y_2O_3 in the 2% BHO DD film affected the film microstructure. This is evidenced in the TEM imaging as the BHO nano-rods are shorter, and interspersed with Y_2O_3 nanoparticles.

The decrease in the anisotropic current density contribution resulting from the additional Y_2O_3 dopants affecting the BHO nano-rods can also be illustrated by employing the theoretical temperature dependence of the current density model developed by Blatter & Nelson, which distinguishes between anisotropic strong and isotropic weak flux pinning (Equation 1). The anisotropic strong contribution is based on columnar pin line disorder, modeled as a cylindrical well and solving the Ginzburg-Landau equations. The isotropic weak contribution's exponential decrease is due to the inefficiency of point like defects (due to oxygen vacancies) to respond to and pin vortex motion due to thermal activation. It manifests as small bundle pinning. Current density data was measured with a field H // c direction of 3 Tesla at 77, 65, 60, 50, 30, 20, 10, and 5 K with the vsm-ppms. The gnuplot fitting program was utilized to determine the fitting parameters $J_c^{is\text{-}weak}(0)$, $J_c^{an\text{-}strong}(0)$, T_0, and T_+. (Table IV) [13]–[16]. As seen in Fig. 3(d), the contribution of the strong flux pinning in the 2% BHO SD film, is decreased in the 2% BHO DD film. The third graph shows that the experimentally measured current density data agrees with the model developed.

$$\underbrace{J_c(T) = J_c^{is-weak}(0)\exp(-T/T_0)}_{\substack{\text{Isotropic Contribution}\\ \text{Weak Flux Pinning}}} + \underbrace{J_c^{an-strong}(0)\exp\left(-3(T/T_+)^2\right)}_{\substack{\text{Anisotropic Contribution}\\ \text{Strong Flux Pinning}}} \quad (4)$$

$J_c(0)$ = current density at 0 K (extrapolated)
T = temperature (K)

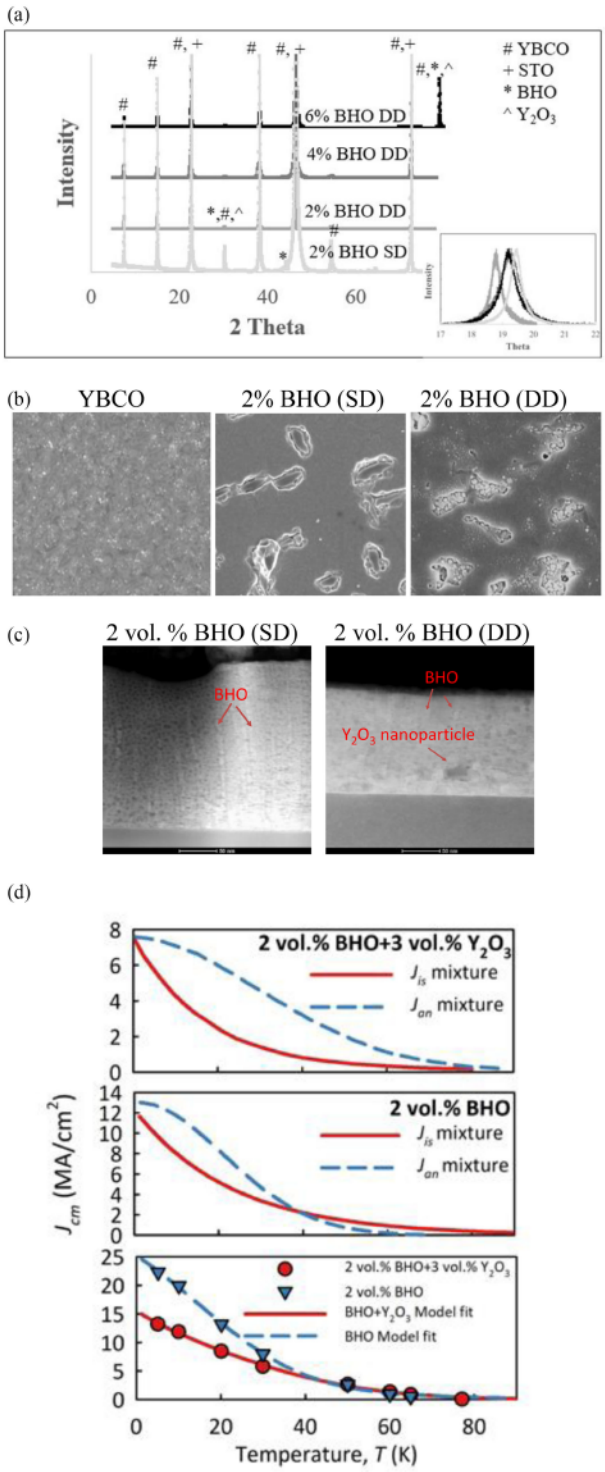

Fig. 3. Microstructure characterization of BHO SD and DD YBCO films (a) XRD analysis, (b) SEM imaging 20kX, (c) TEM imaging, (d) mathematical modeling strong anisotropic flux pinning (-) vs. weak isotropic flux pinning (−) *H//c*,65K, 3T.

T_0, T_+ = curve fitting parameters associated with the energy of the defects.

In conclusion, addition of $BaHfO_3$ to YBCO films, results in epitaxial thin films with nano-rods that contribute to flux pinning and increased current density. The addition of Y_2O_3 also contributes to flux pinning, but interrupts the BHO nano-rod growth. While the Y_2O_3 additions with BHO decrease the highest current density with the field applied in the **c** direction, it decreases the variability in the current density between the c and ab directions. This attribute is an important aspect to consider in applications, such as for HTS wires for motors.

TABLE III
XRD ANALYSIS

Composition	FWHM YBCO (005)	c-lattice parameter YBCO (005) (Å)
2 % BHO DD	0.353	11.7779
4 % BHO DD	0.759	11.7571
6 % BHO DD	0.567	11.7336
2 % BHO SD	0.418	11.7779

TABLE IV
GNUPLOT FITTING PARAMETERS

	$J_c^{\text{iso-weak}}(0)$ (A/cm^2)	$J_c^{\text{an-strong}}(0)$ (A/cm^2)	T_0 (K)	T_+ (K)
2 vol. % BHO + 3 vol. % Y_2O_3	0.790E+07	0.757E+07	17.29	74.38
2 vol. % BHO	1.211E+07	1.305E+07	23.48	51.20

REFERENCES

[1] J. P. F. Feighan, A. Kursumovic, and J. L. MacManus-Driscoll, "Materials design for artificial pinning centres in superconductor PLD coated conductors," *Supercond. Sci. Technol.*, vol. 30, no. 12, Nov. 2017, Art. no. 123001.

[2] K. Matsumoto and P. Mele, "Artificial pinning center technology to enhance vortex pinning in YBCO coated conductors," *Supercond. Sci. Technol.*, vol. 23, no. 1, Dec. 2009, Art. no. 014001.

[3] L. Opherden *et al.*, "Large pinning forces and matching effects in $YBa_2Cu_3O_{7-\delta}$ thin films with $Ba_2Y(Nb/Ta)O_6$ nano-precipitates," *Sci. Rep.*, vol. 18, no. 6, Feb. 2016, Art. no. 21188.

[4] M. A. P. Sebastian *et al.*, "Optimizing flux pinning of YBCO superconductor with dual mixed phase additions," *IEEE Trans. Appl. Supercond.*, vol. 23, no. 3, Jun. 2013, Art. no. 8002104.

[5] V. F. Solovyov *et al.*, "Influence of defect-induced biaxial strain on flux pinning in thick $YBa_2Cu_3O_7$ layers," *Phys. Rev. B* vol. 86, no. 9, Sep. 2012, Art. no. 094511.

[6] H. Zhou *et al.*, "Thickness dependence of critical current density in $YBa_2Cu_3O_{7-\delta}$ films with $BaZrO_3$ and Y_2O_3 addition," *Supercond. Sci Technol.*, vol. 22, no. 8, Jul. 2009, Art. no. 085013.

[7] B. Gautam, S. Chen, M. A. Sebastian, T. Haugan, Z. Xing, and J. Wu, "Mixed artificial pinning centers by single-doping $BaZrO_3$ and double-doping $BaZrO_3$ + Y_2O_3 $YBa_2Cu_3O_{7-x}$ on flat and vicinal substrates," *IEEE Trans. Appl. Supercond.*, vol. 28, no. 4, Jun. 2018, Art. no. 8000104.

[8] M. A. P. Sebastian *et al.*, "Study of the flux pinning landscape of YBCO thin films with single and mixed phase additions $BaMO_3$ Z: M = Hf, Sn, Zr and Z = Y_2O_3, Y211," *IEEE Trans. Appl. Supercond.*, vol. 27, no. 4, Jun. 2017, Art. no. 7500805.

[9] S. Sato *et al.*, "Introducing artificial pinning centers into YBCO thin films to improve surface resistance in a DC magnetic field," *IEEE Trans. Appl. Supercond.*, vol. 23, no. 3, Jun. 2013, Art no. 7200404.

[10] M. Watanebe, S. Sato, K. Sato, K. Ichikawa, A. Saito, and S. Ohshima, "Experimental study in the development of HTS NMR probe," *J. Phys. Conf. Ser.*, vol. 507, Sep. 2013, , Art. no. 012051.

[11] M. Sieger *et al.*, "$BaHfO_3$-doped thick $YBa_2Cu_3O_{7-\delta}$ films on highly alloyed textured Ni-W tapes," *IEEE Trans. Appl. Supercond.* vol. 25, no. 3, Jun. 2015, Art. no. 6602604.

[12] T. Matsushita *et al.*, "Improvement of flux pinning performance at high magnetic fields in $GdBa_2Cu_3O_y$ coated conductors with BHO nano-rods through enhancement of B_{c2}," *Supercond. Sci. Technol.*, vol. 25, no. 12, Oct. 2012, Art. no. 125003.

[13] J. Gutierrez *et al.*, "Strong isotropic flux pinning in solution-derived $YBa_2Cu_3O_{7-x}$ nanocomposite superconductor films," *Nature Mater.*, vol. 6, no. 5, pp. 367–373, May 2007.

[14] J. Gutierrez, T. Puig, and X. Obradors, "Anisotropy and strength of vortex pinning centers in $YBa_2Cu_3O_{7-x}$ coated conductors," *Appl. Phys. Lett.*, vol. 90, no. 16, Apr. 2007, Art. no. 162514.

[15] G. Blatter, M. Feigel'man, V. Geshkenbein, A. Larkin, and V. M. Vinokur, "Vortices in high-temperature superconductors," *Rev. Mod. Phys.*, vol. 66, no. 4, pp. 1125–1388, Oct. 1994.

[16] D. Ertaş and D. R. Nelson, "Irreversibility, mechanical entanglement and thermal melting in superconducting vortex crystals with point impurities," *Phys. C Supercond.*, vol. 272, no. 1, pp. 79–86, Nov. 1996.

[17] A. Feteira, D. C. Sinclair, K. Z. Rajab, and M. T. Lanagan, "Crystal structure and microwave dielectric properties of alkaline-earth hafnates, $AHfO_3$ (A = Ba, Sr, Ca)," *J. Amer. Ceram. Soc.*, vol. 91, no. 3, pp. 893–901, Mar. 2008.

[18] C. P. Bean, "Magnetization of high-field superconductors," *Rev. Mod. Phys.*, vol. 36, no. 1, pp. 31–39, Jan. 1964.

[19] C. P. Bean, "Magnetization of hard superconductors," *Phys. Rev. Lett.*, vol. 8, no. 6, pp. 250–253, Mar. 1962.

[20] J. W. Kell, T. J. Haugan, M. F. Locke, and P. N. Barnes, "Tb and Ce doped Y123 films processed by pulsed laser deposition," *IEEE Trans. Appl. Supercond.*, vol. 15, no. 2, pp. 3726–3729, Jun. 2005.

[21] M. A. Sebastian *et al.*, "Comparison study of the flux pinning enhancement of YBCO superconductor with BZO and BZO + Y_2O_3 mixed phase additions," *IOP Conf. Ser. Mater. Sci. Eng.*, vol. 279, no. 1, Dec. 2017, Art. no. 012031.